GSA Data Repository 2010026 - Simpson

Supplementary explanation of numerical model

The finite element model (Simpson, 2006a) considers two dimensional, plane-strain deformation within a rectangular box, tilted at 5° towards the hinterland, containing three different mechanical phases: air, sediment and indentor, representing a relatively stiff continent (Fig 1B). The indentor is moved to the left at a constant rate, displacing the air and sediment, leading to the formation of a deformed sedimentary wedge. No lateral slip is imposed along the base of the box whereas all other boundaries are free-slip. While sediment can exit the accretionary wedge by flowing under the indentor (depending on the gap thickness), the height of the indentor is such that no sediment can reach its upper surface. Although this setup is similar to that implemented in other studies focusing on accretionary prisms (e.g., Mugnier et al., 1997) it differs from the velocity discontinuity (S-point) boundary condition enabling the formation of a doubly-vergent wedge (Willett et al, 1993). The geometry and characteristics of the indentor (i.e., forward- or backward-dipping backstops, deformable versus non-deformable) can have a large bearing on the prisms and basins that form (e.g., see Persson, 2001). However, because there is still no consensus on which backstop setup best reflects nature, the most simple, vertical rigid indentor was adopted here for simplicity.

The sediment is assumed to exhibit elasto-visco-plastic behavior. Plastic deformation is assumed to be incompressible and is governed by a Mohr-Coulomb law. The air phase is treated as a low density, low-viscosity material whereas the indentor is elastic but behaves essentially rigidly due to a high elastic shear modulus. Dynamic pore pressure effects are neglected but are treated

indirectly by assuming a weak (low viscosity) basal detachment layer. Note also that although natural accretionary prisms are typically submarine, the simulated prisms are subaerial and therefore neglect gravity loads due to an overlying water column. The influence of the water column can be significant at subduction margins where 2.5 km of water is equivalent to approximately 1 km of sediment (see Simpson, 2006b). Thus, in terms of Mohr-Coulomb strength, the deeper the water column, the stronger a rock behaves (due to the additional pressure), neglecting other effects.

Two different mechanisms accounting for surface mass redistribution are included. The first is linear diffusion which is mass conserving and operates over relatively small length scales. The second, described in more in the main text, is hinterland sediment input and long-range transport governed by the horizontal filling (to spill) of local topographic depressions.

Unless stated otherwise, the following parameter values were used in all simulations (omitting those related to air and the rigid indentor): shear modulus = 5×10^9Pa, Poisson's ratio = 0.3, shear viscosity = 10^{35}Pa s, basal shear viscosity = 10^{20}Pa s, thickness of low viscosity basal layer = 500 m, cohesive strength = 50 MPa, angle of internal friction 30^o, basal friction angle = 0^o, rock density = 2500 kg/m^3, surface process diffusivity = 3.6 m^2/yr, convergence rate =20 mm/yr, thickness of subduction window = 600m. Please also note the following points:

1. Although in nature one could expect that preexisting oceanic sediments on the incoming plate have different mechanical properties to the terriginous sediment derived from the adjacent continent deposited during deformation, these differences are neglected here in order to clearly identify differences related to the presence/absence of active sedimentation.

2. The thickness of the basal low-viscosity zone (i.e. 500 m) is far thicker than detachment zones in accretionary prisms which tend to be very sharp. This zone is assumed to be relatively thick in the models for numerical reasons - so that it extends several finite elements away from the no-slip lower boundary. However, even though this basal layer has homogeneous properties, the basal décollement tends to localize along the interface between the basal low-viscosity zone and the overlying sequence and is thus thinner than the basal layer. Please note that although the location of the basal low-viscosity zone is not shown in the figures, it is always present regardless of whether the sediment in the basal zone is preexisting or derived from hinterland sediment input. Please also note that no part of the basal low viscosity layer is ever permitted to be thrust into any part of the overlying wedge.

3. The shear viscosity of the wedge above the low-viscosity basal layer is set to an arbitrary elevated value of 10^{35}Pa s. This simply ensures that the wedge (above its basal layer) behaves as an elastic-plastic material with negligible viscous deformation.

4. Although the basal friction angle is zero, a non-zero cohesion value ensures a finite rock strength on the basal detachment. The basal detachment zone thus behaves as a pressure-independent, viscous Von-Mises material.

5. All models include strain weakening of cohesion, whereby the cohesion strength decreases nonlinearly as a function of the finite strain. Note that this implies that once some plastic strain is accumulated, the cohesion value will drop abruptly (essentially to zero after approximately 2% of strain) and remain low thereafter even if deformation later shifts elsewhere, since the finite plastic strain will remain. Note that the initial

cohesive rock strength has a relatively elevated value which was chosen in order to have ‘sharp’ shear zones. Strain weakening is not necessary in order to have shear localization but is also included to enhance the appearance of shear zones.

Most experiments were run for a total time of 2.22 million years (i.e., 44.4 km of convergence).

References Cited

Mugnier, J.L., Baby, P., Colletta, B., Vinour, P., Bale, P., and Leturmy, P., 1997, Thrust geometry controlled by erosion and sedimentation: A view from analogue models: Geology, v. 25, p. 427-430.

Persson, K.S., 2001, Effective indentors and the development of double-vergent orogens: Insights from analogue sand models, in Koyi, H.A and Mancktelow, N.S., eds., Tectonic modeling: A volume in Honor of Hans Ramberg: Boulder, Colorado, Geological Society of America Memoir 193, 191-206.

Simpson, G.D.H., 2006a, Interactions between fold-thrust belt deformation, foreland flexure and surface mass transport: Basin Research, v. 18, p. 125-143.

Simpson, G.D.H., 2006b, How and to what extent does the emergence of orogens above sea level influence their tectonic development? Terra Nova, v. 18, 447-451, doi: 10.1111/j.1365-3121.2006.00711.x

Willett, S., Beaumont, C., and Fullsack, P., 1993, Mechanical model for the tectonics of doubly vergent compressional orogens: Geology, v. 21, p. 371-374.

Captions

Video DR1: Video of a numerical model (see Fig 3, main text) showing the formation of an accretionary wedge fed by a time-varying sediment supply rate. The sediment supply rate introduced at the top of the wedge oscillates in a stepwise manner between 48 km^2/my and 4.8 km^2/my with a period of 0.55 my, while the flux of sediment exiting the wedge by subduction is maintained at 12 km^2/my. The upper panel shows the time-varying sediment supply rate (the current supply rate is indicated by a red dot) whereas the lower panel illustrates deformed synthetic stratigraphy where colors alternate at regular time intervals (60 ky). When the sediment input exceeds output due to subduction, the wedge has a low surface slope and a thick, wide trench due to high sedimentation rates. A 10 fold reduction in the sediment supply rate starves the trench and wedge of sediment causing it to narrow and steepen (i.e., towards becoming critical).

Figure DR1: Diagrams illustrating how wedge-top sedimentation for the simulation presented in Fig 2b of the main text influences stresses in the wedge, causing it to become supercritical. A: Plot showing the maximum stress σ_1 (dotted line) and the minimum stress σ_3 (solid line) at a fixed point (with respect to material not position) as a function of depth for three different times, 1.1 my (PA), 1.65 my (PB), and 2.2 my (PC). PA refers to the location of the upper surface of the wedge before significant wedge top sedimentation, whereas PB and PC (located 15 km from the backstop in Fig 2b) refer to the upper surface at later times after a significant amount of wedge-top sedimentation. Also shown is the approximate position of the maximum stress at each time, computed from the Mohr-Coulomb envelope (labeled Mohr envelope and shown as a dashed line). Stresses are negative in compression. The Mohr diagrams in B and C illustrate schematically how stresses in the wedge respond to wedge-top sedimentation and tectonic loading, respectively (assuming a convergent tectonic regime where is vertical σ_3 and is σ_1 horizontal. Note that due to sedimentation, PA becomes buried with time under PB and PC. Initially (time PA), the entire upper part of the wedge is in a critical state - i.e, stressed to the failure envelope (solid circle in B). Thereafter (times PB and PC), wedge top sedimentation increases the vertical (minimum) stress (dashed circle in B), at a rate which exceeds the increase in the maximum stress from horizontal convergence (C). The net effect is to decrease the differential stress in the upper part of the wedge, driving the stress state into the stable field.

A. Stresses in wedge with sedimentation

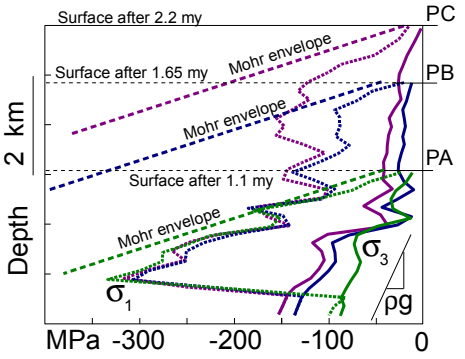

B. Unloading due to sedimentation

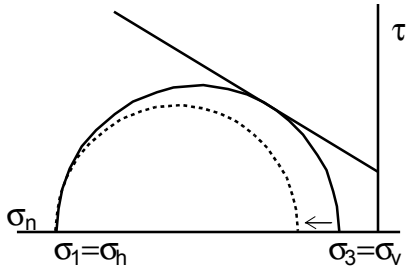

C. Tectonic loading to failure

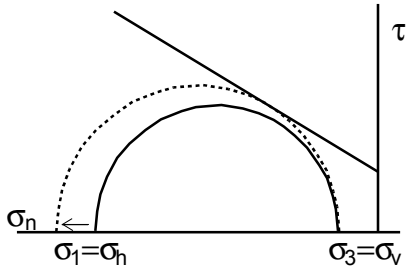

Fig. DR1 - Simpson